Model-based Fault Diagnostics of Servo Valves

Turki Haj Mohamad[1], Foad Nazari[2], and Chandrasekhar Nataraj[3]

[1,2,3] *Villanova Center for Analytics of Dynamic Systems (vcads.org),*
Villanova University, Villanova, PA 19085, USA
thajmoha@villanova.edu
foad.nazari@villanova.edu
c.nataraj@villanova.edu

Abstract

This paper presents the application of the Extended Phase Space Topology (EPST) method in model-based diagnostics of nonlinear systems. A detailed nonlinear mathematical model of a servo electro-hydraulic system has been used to demonstrate the procedure. Two faults have been considered associated with the servo valve including the increased friction between spool and sleeve and the degradation of the permanent magnet of the valve armature. The faults have been simulated in the system by the variation of the corresponding parameters in the model and the effect of these faults on the output flow response has been investigated. A regression-based artificial neural network has been developed and trained using the EPST extracted features to estimate the original values of the faulty parameters and to identify the severity of the faults in the system.

1. Introduction

Electro-hydraulic servo valves have generated considerable research interest due to their high degree of accuracy in regulating and controlling fluid flow in a wide variety of applications such as hydro-electric power plants, aircraft engines and manufacturing. Servo valves consist of complex components that handle precise and sensitive tasks, such as starting or stopping a flow, modifying the velocity or changing the pressure, etc. Any deviation of the system components' parameters or dimensions may lead to instability or system failure. Hence, it is important to develop effective diagnostic techniques to constantly monitor the performance of such systems and to identify any faults, including their locations and severity levels.

Fault detection and diagnostic techniques can be classified into two main categories: data driven approaches and model-based approaches. Data driven approaches are based on sig-nal processing techniques that are performed on data measured from the system. These techniques strive to extract features to indicate the status of the system. Model-based approaches use physics, represented by mathematical models of the system, in order to detect faults.

One of the main approaches in model-based fault detection is to use parameter estimation techniques (Isermann, 1982, 1984; Frank, Ding, & Koppen-Seliger, 2000). Parameter estimation is the main scope of this research, which is based on estimating and comparing the parameters of a defective system with the parameters of a healthy system. The main thesis is that the change in the system parameters is usually associated with the system defects (Isermann, 2005; Baskiotis, Raymond, & Rault, 1979; Kappaganthu & Nataraj, 2011; Liu, Zhang, Liu, & Yang, 2000).

Due to the highly nonlinear characteristics of servo valves, it is essential to use techniques that can perform effectively in different domains of the nonlinear response. This paper presents a continuation of our past work (Samadani, Kwuimy, & Nataraj, 2014), in which the application of recurrence plots (RPs) and recurrence quantification analysis (RQA) were introduced. Despite the success of the previous method in parameter estimation, it can be time consuming and computationally demanding, which makes it hard for it to be applied in an automated manner or for it to be integrated into a control system. Thus, this investigation presents a new approach for parameter estimation-based diagnostics of nonlinear systems, based on the extracted information from the nonlinear response.

In an earlier work, we presented the method of Phase Space Topology (PST) (Samadani, Kwuimy, & Nataraj, 2015, 2013), which is based on transforming the phase space into the density space and characterizing the density with quantitative measures. It was shown that, depending on the geometry and shape of the phase space, the density profile contains peaks of various heights and sharpness at multiple locations. The properties of the peaks in the density distri-

bution, including the location, height and sharpness of the peaks, were used as features in the initial approach. The need to search for the peaks in the density distributions makes the PST difficult or sometimes even impractical to implement, especially for systems with noisy or more complex phase space patterns. We next improved this approach with Extended Phase Space Topology (EPST) (Mohamad & Nataraj, 2017; Samadani, Mohamad, & Nataraj, 2016; Mohamad, Samadani, & Nataraj, n.d.; Mohamad, Kwuimy, & Nataraj, 2017), which will be discussed in detail in Section 3. The EPST method is based on characterizing the topology of the density distribution of the response signal, which is then expanded in a series of Legendre polynomials. The coefficients of the orthogonal polynomials are subsequently used as features for a machine learning algorithm to estimate the system parameters. The present paper extends that approach to be used as a parameter estimation model-based technique.

Model-based condition monitoring requires a mathematical representation of the system that can describe the behavior of the system (here, the servo valve). Thus, a detailed nonlinear mathematical model has been used to simulate the system response under various conditions. Faults can be defined as undesired deviations of a characteristic property or a system parameter from the standard acceptable domain, which causes limitations in achieving a planned task (Isermann, 1984). Two faults have been considered associated with the servo valve: the increased friction between spool and sleeve and the degradation of the permanent magnet of the valve armature. Various electrical current signals, i.e., periodic, biperiodic and quasi-periodic, are used as inputs to the servo valve system. The EPST method is then performed on the output flow of the servo valve to identify dynamical changes in the system associated with the faults. Finally, an artificial neural network (ANN) is trained for mapping of the feature space to the parameter space.

The remaining parts of this paper are organized as follows. In Section 2, a detailed mathematical model of the electrohydraulic valve has been derived. In Section 3, the definition of EPST has been presented. Section 4 presents a parametric analysis for the servo valve system. In Section 5, the parametric estimation algorithm is discussed along with the results. Finally, Section 6 concludes the paper.

2. MODELING OF THE ELECTRO-HYDRAULIC SERVO SYSTEM

A detailed dynamical model of a two-stage servo valve system (shown in Fig. 1) with mechanical feedback has been used in the analysis. Only the final equations are presented here. The detailed explanation of the model derivations can be found in (Samadani, Behbahani, & Nataraj, 2013; Rabie, 2009; Gordić, Babić, & Jovičić, 2004). The definition of sys-
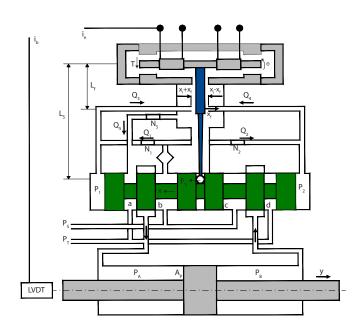

Figure 1. Functional schematic of the electro-hydraulic servo system

tem states and parameters along with nominal values of the parameters have been presented in the nomenclature.

Neglecting the effect of the magnetic hysteresis, the net torque on the armature is given by the following expression.

$$T = K_i i_e \tag{1}$$

where, the coefficient K_i can be calculated by:

$$K_i = \frac{N\lambda_p \mu_o AL}{2x_o^2} \tag{2}$$

The motion of the armature and the elements attached to it is described by the following equations:

$$T = J\frac{d^2\theta}{dt^2} + f_\theta\frac{d\theta}{dt} + K_T\theta + T_L + T_P + T_F \tag{3}$$

$$T_P = A_f(P_2 - P_1)L_f \tag{4}$$

where,

$$A_f = \frac{\pi}{4}d_f^2 \tag{5}$$

The feedback torque depends on the displacement of the spool and the angle of the flapper and can be given by:

$$T_F = F_S L_S = K_S(L_S\theta + x)L_S \tag{6}$$

The rotational displacement of the flapper is limited mechanically by the jet nozzles. When the flapper reaches any of the side jet nozzles, a counter torque T_L is applied to it which can

be calculated by the following equation:

$$T_L = \begin{cases} 0, & |x_f| < x_i \\ R_s \frac{d\theta}{dt} - (|x_f| - x_i) K_{Lf} L_f \mathrm{sign}(x_f), & |x_f| > x_i \end{cases} \tag{7}$$

where,

$$x_f = L_f \theta \tag{8}$$

The flow rates through the flapper valve restrictions are given by the following equations:

$$Q_1 = C_D A_o \sqrt{\frac{2}{\rho}(P_s - P_1)} = C_{12}\sqrt{(P_s - P_1)} \tag{9}$$

$$Q_2 = C_D A_o \sqrt{\frac{2}{\rho}(P_s - P_2)} = C_{12}\sqrt{(P_s - P_2)} \tag{10}$$

$$Q_3 = C_d \pi d_f (x_i + x_f) \sqrt{\frac{2}{\rho}(P_1 - P_3)}$$
$$= C_{34}(x_i + x_f)\sqrt{(P_1 - P_3)} \tag{11}$$

$$Q_4 = C_d \pi d_f (x_i - x_f) \sqrt{\frac{2}{\rho}(P_2 - P_3)}$$
$$= C_{34}(x_i - x_f)\sqrt{(P_2 - P_3)} \tag{12}$$

$$Q_5 = C_d A_s \sqrt{\frac{2}{\rho}(P_3 - P_T)} = C_5\sqrt{(P_3 - P_T)} \tag{13}$$

By using the continuity equation for the chambers of the flapper valve, the following expressions can be deduced:

$$Q_1 - Q_3 + A_s \frac{dx}{dt} = \frac{V_o - A_s x}{B} \frac{dP_1}{dt} \tag{14}$$

$$Q_2 - Q_4 - A_s \frac{dx}{dt} = \frac{V_o + A_s x}{B} \frac{dP_2}{dt} \tag{15}$$

$$Q_3 + Q_4 - Q_5 = \frac{V_3}{B} \frac{dP_3}{dt} \tag{16}$$

The motion of the spool is governed by the following equations.

$$A_s(P_2 - P_1) = m_s \frac{d^2 x}{dt^2} + f_s \frac{dx}{dt} + F_j + F_s \tag{17}$$

$$F_j = \begin{cases} \left(\frac{\rho Q_b^2}{C_c A_b} + \frac{\rho Q_d^2}{C_c A_d}\right)\mathrm{sign}(x) & \text{for } x > 0 \\ \left(\frac{\rho Q_a^2}{C_c A_a} + \frac{\rho Q_c^2}{C_c A_c}\right)\mathrm{sign}(x) & \text{for } x < 0 \end{cases} \tag{18}$$

Ignoring the effect of transmission lines between the valve and the symmetrical hydraulic cylinder, the flow rates through

the valve restriction areas are given by:

$$Q_a = C_d A_a(x)\sqrt{\frac{2}{\rho}(P_A - P_T)} \tag{19}$$

$$Q_b = C_d A_b(x)\sqrt{\frac{2}{\rho}(P_s - P_A)} \tag{20}$$

$$Q_c = C_d A_c(x)\sqrt{\frac{2}{\rho}(P_s - P_B)} \tag{21}$$

$$Q_d = C_d A_d(x)\sqrt{\frac{2}{\rho}(P_B - P_T)} \tag{22}$$

$$\tag{23}$$

The area of the valve restrictions are given by:

$$\begin{cases} A_a = A_c = \omega c \\ A_b = A_d = \omega\sqrt{(x^2 + c^2)} \end{cases} \quad \text{for } x \geq 0 \tag{24}$$

$$\begin{cases} A_a = A_c = \omega\sqrt{(x^2 + c^2)} \\ A_b = A_d = \omega c \end{cases} \quad \text{for } x \leq 0 \tag{25}$$

Considering the internal leakage and neglecting the external leakage, the following equations can be obtained by applying the continuity equation to the cylinder chambers.

$$Q_b - Q_a - A_P \frac{dy}{dt} - \frac{(P_A - P_B)}{R_i} = \frac{(V_c + A_p y)}{B} \frac{dP_A}{dt} \tag{26}$$

$$Q_c - Q_a d + A_P \frac{dy}{dt} - \frac{(P_A - P_B)}{R_i} = \frac{(V_c - A_p y)}{B} \frac{dP_B}{dt} \tag{27}$$

Finally, the equation of motion for the cylinder piston is given by:

$$A_P(P_A - P_B) = m_p \frac{d^2 y}{dt^2} + f_P \frac{dy}{dt} + K_b y \tag{28}$$

3. FEATURE EXTRACTION METHOD

Let $X = (x_1, x_2, ..., x_n)$ be an independent and identically distributed sample data drawn from a distribution with an unknown density function Ψ. The shape of this function can be estimated by its kernel density estimator ($\hat{ }$ indicates that it is an estimate, and h indicates that its value can depend on h).

$$\hat{\Psi}_h(x) = \frac{1}{nh}\sum_{i=1}^{n}\Gamma\left(\frac{x - x_i}{h}\right) \tag{29}$$

where, $h > 0$ is a smoothing parameter called the bandwidth, and $\Gamma(.)$ is the kernel function which satisfies the following requirements.

$$\int_{-\infty}^{\infty}\Gamma(u)\,du = 1 \tag{30}$$

$$\Gamma(-u) = \Gamma(u) \,\forall u \tag{31}$$

There is a range of kernel functions that can be used, including uniform, triangular, biweight, triweight, Epanechnikov, normal, etc. Due to its conventional and convenient mathematical properties, we use the standard normal density function in our approach, defined as the following:

$$\Gamma(u) = \frac{1}{\sqrt{2\pi}} e^{-\frac{1}{2}u^2} \tag{32}$$

Let x be a state of the system and $y_d = \hat{f}_h(x)$, its density computed using the kernel density estimator. y_d is then approximated with Legendre orthogonal polynomials. Legendre polynomials can be directly obtained from Rodrigues' formula which is given by:

$$\Phi_m(x) = \frac{1}{2^m m!} \frac{d^m}{dx^m} \left[(x^2 - 1)^m \right], \quad m = 0, 1, 2, \ldots \tag{33}$$

It can also be obtained using Bonnet's recursion formula:

$$(m+1)\Phi_{m+1}(x) = (2m+1)x\Phi_m(x) - m\Phi_{m-1}(x) \tag{34}$$

where the first two terms are given by:

$$\Phi_0(x) = 1, \quad \Phi_1(x) = x \tag{35}$$

The coefficients of the Legendre polynomials are obtained by using the least squares method assuming the following linear regression model:

$$\Psi(x, \beta) = \sum_{j=1}^{m} \beta_j \Phi_j(x) \tag{36}$$

Letting

$$X_{ij} = \frac{\partial \Psi(x_i, \boldsymbol{\beta})}{\partial \beta_j} = \Phi_j(x_i), \tag{37}$$

the estimated coefficients are given by:

$$\hat{\beta} = (X^T X)^{-1} X^T y_d \tag{38}$$

The coefficients $\hat{\beta}$ constitute the features in our approach that can be used in classification or regression problems. The approximated density using Legendre Polynomials is then calculated using the following:

$$\Psi_a = X\hat{\beta} \tag{39}$$

Root mean square error (RMSE) and Pearson's correlation coefficient (PCC) were calculated to compute the quality of the fit using the following equations:

$$\text{RMSE} = \sqrt{\frac{1}{N} Z Z^T}, \quad \text{PCC} = \frac{\sigma_d^T \sigma_a}{\sqrt{(\sigma_d^T \sigma_d)(\sigma_a^T \sigma_a)}} \tag{40}$$

where, $Z = (y_d - \Psi_a)$ is the residual vector, N is the number of points in the density function, $\sigma_d = (y_d - E\{y_d\})$ and $\sigma_a = (\Psi_a - E\{\Psi_a\})$. $E\{.\}$ is the expected value.

4. PARAMETRIC ANALYSIS

For identification of faults, we propose to inject a pre-specified signal to the system and to compare the system response with the healthy condition response. In this study, an electrical current signal is applied to the servo valve system after which the output flow of the servo valve is measured for one second. Note that all analysis were performed using the mathematical model without any experimental data.

To analyze the effectiveness of the approach, three signals were used as inputs for the servo valve as follows:

- Periodic input signal

$$i = 0.01 \sin(50t) \tag{41}$$

- Bi-Periodic input signal

$$i = 0.01 \sin(50t) + 0.005 \sin(75t) \tag{42}$$

- Quasi-Periodic input signal

$$i = 0.01 \sin(50t) + 0.005 \sin(50\pi t) \tag{43}$$

There are many parameters that can be monitored in typical electro-hydraulic systems. In this study, as mentioned earlier, two faults have been considered: (1) the degradation of the permanent magnet of the valve armature, represented by the change of the coefficient K_i, and (2) the increased friction between spool and sleeve, represented by the change of the spool friction coefficient f_S.

In equations 44 and 45, CK_i and Cf_s are defined to show variation of K_i and f_s from the healthy condition.

$$CK_i = \frac{K_i}{\overline{K}_i} \tag{44}$$

$$Cf_s = \frac{f_s}{\overline{f}_s} \tag{45}$$

where, $\overline{K}_i$ and $\overline{f}_s$ denote the values of K_i and f_s for the healthy condition and are equal to 0.559 Nm/A and 3.05 Ns/m, respectively. When CK_i or Cf_s are close to 1, the system can be considered to operate in healthy condition. In addition to the healthy condition (CK_i and Cf_s are equal to 1), eight faulty conditions are considered in this section. Four of the conditions are caused by decreasing CK_i by 20%, 40%, 60% and 80%. The remaining four conditions are caused by increasing Cf_s 5, 10, 20 and 30 times.

The effect of the five cases of the coefficient CK_i ($CK_i = \{1, 0.8, 0.6, 0.4, 0.2\}$), on the output flow of the servo valve for three input signals are compared in Fig. 2. As is clearly seen in this figure, for all three input cases, a decrease of CK_i

results in a decrease of the output flow amplitude of the servo valve. It is also concluded that the output flow is very sensitive to the variation of CK_i, because any change in CK_i affects the time response of the system.

In Fig. 3, the time response of the servo valve system for three input signals and various values of Cf_s are presented. Five cases of the Cf_s parameter were studied ($Cf_s = \{1, 5, 10, 20, 30\}$). It can be seen that the effect of Cf_s on the time response of the system is not as easily observed as the response for changing CK_i. To show how the output flow of the valve is affected by Cf_s, some main points of the graphs are magnified and added to the main figures. From the magnified sections, it is concluded that increasing the parameter Cf_s results in a decrease of the amplitude of output flow at certain time ranges and an increase of the output flow amplitude at other ranges. This indicates that changing Cf_s affects the output flow in a nonlinear fashion. In general, the change in K_i or f_s affects the output flow of the servo valve system. This indicates that the output flow has valuable information about the parameters K_i and f_s, which can be used in solving the inverse problem of estimating the parameters using all provided information that is contained within the output flow of the servo valve.

5. FAULT IDENTIFICATION AND SEVERITY ANALYSIS

The previous section illustrates how the time response of the system is affected by the change of f_s and K_i parameters and how the response for the f_s parameter changes in a nonlinear fashion. In this section, the values of f_s and K_i parameters are predicted based on the time response of the system. In order to capture all available information provided by the output flow of the servo valve, the EPST method is applied. A summary of the proposed method is shown in Fig. 4.

The EPST extracted features were used to train two artificial neural networks (ANNs). ANNs are a form of a multi-processor system with a high degree of inter-connection simple processing elements, simple scalar messages and adaptive interaction between elements. A multi-layer feed forward (MLFF) ANNs, which is one of the most popular type of ANNs is used in this study. The structure of the MLFF network includes an input layer, one or more hidden layers and an output layer, in which each layer consists of some neurons.

In this work, the Back-Error Propagation (BEP) algorithm was employed in order to minimize the error of the ANN model. The BEP is one of the most widely used learning algorithm of MLFF-ANNs. In the trained ANNs, the activation functions for the neurons of hidden and output layers were Tansig and linear, respectively. Two distinct ANNs were created with ten neurons in the input layer and a single neuron in the output layer. The inputs of the ANNs were selected to be the first ten coefficients of the Legendre polynomials. The target outputs of first and second ANNs were Cf_s and
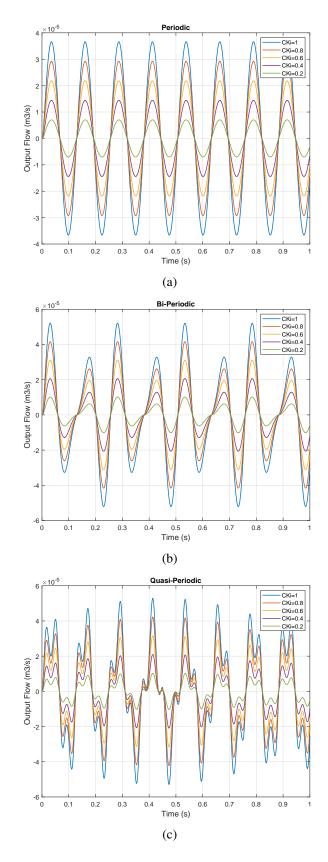

Figure 2. Time response of the system for (a): periodic, (b): bi-periodic and (c): quasi-periodic inputs to the servo valve for various values of CK_i
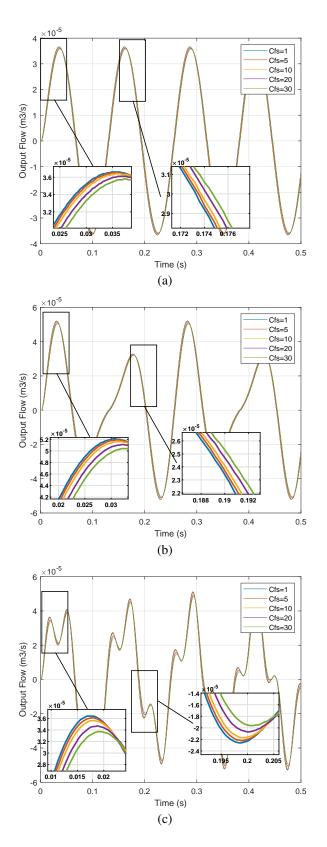
5

(a)

(b)

(c)

Figure 3. Time response of the system for (a): periodic, (b): bi-periodic and (c): quasi-periodic inputs to the servo valve for various values of Cf_s
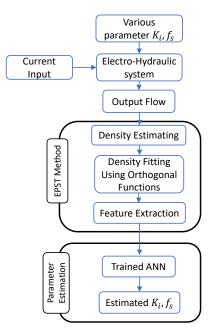

Figure 4. The process of the parameter estimation method

CK_i, respectively. The data was obtained by random selection of the f_s and K_i values in the intervals of [1, 100] and [0.1, 0.6], respectively. Simulation of the servo valve system was then performed and the response features, i.e., Legendre polynomial coefficients, were computed at each time. A total number of 291 samples was used for training, validation and testing of the model. In the BEP training procedure, 70%, 20% and 10% of data were used for training, testing and verification, respectively. An additional 9 samples were used to compare the predicted and the actual values of the K_i and f_s parameters. All data were applied to ANNs in normalized form. The ANNs were trained and tested with three various set of data obtained from periodic, bi-periodic and quasi-periodic inputs of the servo-valve system.

To predict the f_s and K_i parameters, five hidden layer configurations (i.e., 5, 10, 15, 20 or 25 neurons) were considered. Using the obtained data of the quasi-periodic input, a comparison between the different hidden layer configurations was performed. The minimum error was considered to select the optimum neuron number in the hidden layer. The obtained results are presented in Fig. **??**. As can be seen, the least error values in prediction of K_i and f_S were obtained with 15 and 5 neurons in the hidden layer, respectively. The rest of the analyses were performed by considering the obtained optimum neuron numbers for ANNs hidden layer.

The performances of the trained ANN models to predict K_i and f_s parameters for periodic input are shown in Fig. 5. In the training procedure, the number of epochs was assumed to be 400. For various input signals the trained ANN was capable of predicting the K_i and f_s values with high accu-
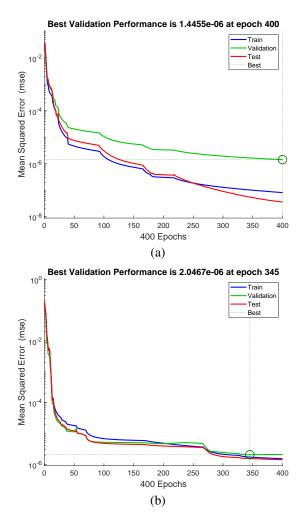
6

(a)

(b)

Figure 5. Training performance of ANNs in prediction of periodic input for a) K_i and b) f_s

racy. This is represented in the performance plots by very low validation and test errors. For example, predicting K_i for a periodic input achieved misprediction rate of $1.44\,\mathrm{e}{-06}$ for the validation samples. In addition, Figure. 6 illustrates the regression plots of the network outputs with respect to targets along the regression values for periodic input. Ideally, the regression value should be close to 1 and the data in the regression plot should fall along a $45°$ line for a perfect fit. As can be seen in this figure, all the points have fallen along the $45°$ line and the regression values are equal or close to 1, which indicates an accurate mapping of the feature space to the parameter space.

Finally, the predicted results are compared with the actual values in Table 1. As can be calculated from the prediction results presented in Table 1, the average prediction error for K_i and f_s are 0.07% and 0.63%, respectively. This shows that the proposed method has a very good ability to predict the original parameters of the system. Although the parametric

analysis showed that the effects of f_s on time response of the system was nonlinear and not as easily observed as K_i, the EPST method was able to predict its value for various input signals and on a wide range with 99.37% accuracy. The EPST parameter estimation algorithm is virtually perfect in predicting the K_i value with 99.93% accuracy.

6. CONCLUSION

We used the Extended Phase Space Topology (EPST) method for model-based fault detection and diagnostics of an electro-hydraulic system. It was shown that the nonlinear response of the system contains valuable information about the system that can be used for this purpose. The analyses were performed with the assumption that only the output response of the system (here output flow of the valve) is available. A parameter analysis was performed on the system in order to study the relationship between changing K_i and f_s parameters and the system response. It was shown that K_i affects the system response linearly where increasing the parameter leads to an increase in the output flow amplitude. On the other hand, changing f_s has a nonlinear relationship to the output flow of the system. It was demonstrated that these dynamical changes can be detected by the EPST method. Finally, two artificial neural network was trained using the EPST features to estimate the faulty parameters of the system. It was shown that the EPST features can be used as effective indicators for characterizing the nonlinear response of the system even in the multi-periodic or quasi-periodic domain with complex nonlinearities.

In this study, the proposed method was only applied to numerical data obtained from the mathematical model of the system. Although the results were promising, there is no guarantee that we can obtain the same prediction accuracy for real experimental data. Hence, it is of importance to confirm the effectiveness of the approach with experimental analysis. In addition, only two parametric defects (defects due to change of parameter values) were considered in this paper, whereas in real world applications we might have multiple parametric defects in the system or even defects of the type that can change the structure of the mathematical model of the system.
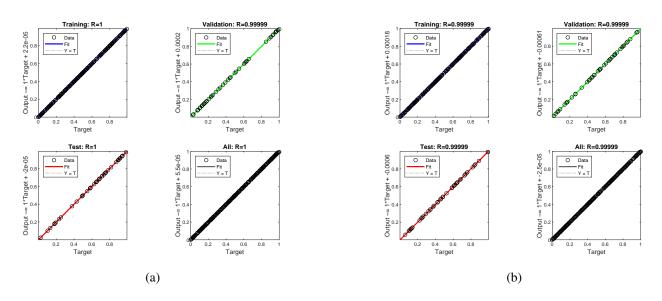
(a)   (b)

Figure 6. Training regression of ANNs in prediction of periodic input for a) K_i b) f_s

Table 1. ANNs fault identification results

No		Actual	Periodic		Bi-Periodic		Quasi-Periodic	
		Value	Value	Error%	Value	Error%	Value	Error%
1	K_i	0.5001	0.5000	0.02	0.5003	0.04	0.5004	0.04
	f_s	81.0000	80.9802	0.02	81.0352	0.04	80.9280	0.09
2	K_i	0.1934	0.1934	0.01	0.1929	0.27	0.1934	0.03
	f_s	27.0000	26.5399	1.70	26.3674	2.34	27.0846	0.31
3	K_i	0.5646	0.5642	0.08	0.5649	0.05	0.5654	0.13
	f_s	49.0000	48.9866	0.03	48.8029	0.40	49.0284	0.06
4	K_i	0.1828	0.1828	0.04	0.1826	0.10	0.1828	0.00
	f_s	70.0000	69.9075	0.13	69.9971	0.00	69.9037	0.14
5	K_i	0.1728	0.1729	0.08	0.1724	0.21	0.1728	0.04
	f_s	25.0000	24.4414	2.23	24.3327	2.67	25.1959	0.78
6	K_i	0.1482	0.1481	0.07	0.1486	0.27	0.1486	0.28
	f_s	35.0000	34.8031	0.56	35.5636	1.61	35.4071	1.16
7	K_i	0.3234	0.3234	0.00	0.3234	0.01	0.3234	0.01
	f_s	67.0000	66.9028	0.15	67.1100	0.16	67.1874	0.28
8	K_i	0.5524	0.5523	0.03	0.5525	0.00	0.5525	0.01
	f_s	63.0000	63.1198	0.19	62.6932	0.49	62.6613	0.54
9	K_i	0.4575	0.4575	0.01	0.4576	0.01	0.4575	0.00
	f_s	44.0000	43.8932	0.24	44.0651	0.15	44.1911	0.43
Mean Error %	K_i		0.04		0.11		0.06	
	f_s		0.58		0.87		0.42	

ACKNOWLEDGMENT

NOMENCLATURE

Electro-Hydraulic Servo System

Symbol	Description	Unit	Value
a	Width of spool edges	m	4e-03
A	Area of air gap	m^2	
A_5	Drain orifice area	m^2	
A_L	Area of the flow between spool and sleeve edges	m^2	
A_o	Orifice area	m^2	
$A_{a'}$, $A_{b'}$, $A_{c'}$, and $A_{d'}$	Spool valve restrictions areas	m^2	
A_P	Piston area	m^2	7e-04
A_s	Spool cross-sectional area	m^2	
b	Width of sleeve slots	m	4e-03
B	Bulk modulus of oil	Pa	1.5e09
c	Spool radial clearance	m	2e-06
C_c	Contraction coefficient		
C_d and C_D	Discharge coefficients		0.661
d_f	Flapper nozzle diameter	m	5e-04
d_5	Diameter of return orifice	m	6e-04
d_s	Spool diameter	m	4.6e-03
f_θ	Armature damping coefficient	Nms/rad	0.002
F_j	Hydraulic momentum force	N	
f_p	Piston friction coefficient	Ns/m	1000
f_s	Spool friction coefficient	Ns/m	3.05
F_s	Force acting at the extremity of the feedback spring	N	
H	Magneto-motive force per unit length	A/m	
i_b	Feedback current	A	
i_c	Control current	A	
i_e	Torque motor input current	A	
J	Moment of inertia of rotating part	Nms^2	5e-07
K_b	Load coefficient	N/m	0
K_{FB}	Feedback gain	A/m	1
K_{Lf}	Equivalent flapper seat stiffness	N/m	1e6
K_i	Current-torque gain	Nm/A	0.559
K_s	Stiffness of the feedback spring	N/m	900
K_T	Stiffness of flexure tube	Nm/rad	10.68
K	Rotational angle-torque gain	Nm/rad	9.45e-4
L	Armature length	m	0.029
L_f	Flapper length	m	0.009
L_s	Length of the feedback spring and flapper	m	0.03
L_{sp}	Length of spool land	m	1.5e-02
m_p	Piston mass	kg	5
m_s	Spool mass	kg	0.2
P_1	Pressure in the left side of the flapper valve	Pa	
P_2	Pressure in the right side of the flapper valve	Pa	
P_3	Pressure in the flapper valve return chamber	Pa	
P_A and P_B	Hydraulic cylinder pressures	Pa	
P_s	Supply pressure	Pa	1.2e7
P_T	Return line pressure	Pa	0
Q	Flow rate	m^3/s	
Q_1	Flow rate in the left orifice	m^3/s	
Q_2	Flow rate in the right orifice	m^3/s	
Q_3	Left flapper nozzle flow rate	m^3/s	
Q_4	Right flapper nozzle flow rate	m^3/s	
Q_5	Flapper valve drain flow rate	m^3/s	
Q_a, Q_b, Q_c, and Q_d	Flow rates through the spool valve restrictions	m^3/s	
R_i	Resistance to internal leakage	Ns/m^5	1e20
R_s	Flapper seat damping coefficient	Nms/rad	5000
T	Torque of electromagnetic torque motor	Nm	
T_F	Feedback torque	Nm	
T_L	Torque due to flapper displacement limiter	Nm	
T_P	Torque due to the pressure forces	Nm	
V_3	Volume of the flapper valve return chamber	m^3	5e-06
V_c	Half of the volume of oil filling the cylinder	m^3	1e-04
V_o	Initial volume of oil in the spool side chamber	m^3	2e-06
x	Spool displacement	m	
x_a	Displacement of the armature end	m	
x_f	Flapper displacement on the level of the jet nozzles	m	
x_i	Flapper displacement limit	m	3e-05
x_o	Length of the air gap in the neutral position of armature	m	3e-04
λ	Magneto-motive force	A	
λ_p	Magneto-motive force of the permanent magnet	A	66.75
μ	Permeability	Vs/Am	
μ_o	Permeability of the air	Vs/Am	4e-07
μ_r	Relative permeability		
ρ	Oil density	kg/m^3	867
ω	Width of ports on the valve sleeve	m	0.014

θ	Armature rotation angle	rad

EPST Method

$\Gamma(.)$	Kernel function
Φ_m	Legendre polynomial of order m
Ψ	Unknown density distribution for a given data
$y_d, \hat{\Psi}$	Estimated kernel density distribution for a given data
Ψ_a	Approximated density distribution for a given data using Legendre polynomials
h	Bandwidth
β	Legendre polynomial coefficients
Z	Residual vector

REFERENCES

Baskiotis, C., Raymond, J., & Rault, A. (1979). Parameter identification and discriminant analysis for jet engine machanical state diagnosis. In *18th IEEE Conference on Decision and Control including the Symposium on Adaptive Processes* (Vol. 18, pp. 648–650).

Frank, P., Ding, S. X., & Koppen-Seliger, B. (2000). Current developments in the theory of FDI. In *Proceedings of SAFEPROCESS* (Vol. 1, pp. 16–27).

Gordić, D., Babić, M., & Jovičić, N. (2004). Modelling of spool position feedback servovalves. *International Journal of Fluid Power*, *5*(1), 37–51.

Isermann, R. (1982). Parameter adaptive control algorithms–a tutorial. *Automatica*, *18*(5), 513–528.

Isermann, R. (1984). Process fault detection based on modeling and estimation methodsa survey. *automatica*, *20*(4), 387–404.

Isermann, R. (2005). Model-based fault-detection and diagnosis–status and applications. *Annual Reviews in Control*, *29*(1), 71–85.

Kappaganthu, K., & Nataraj, C. (2011). Feature selection for fault detection in rolling element bearings using mutual information. *Journal of vibration and acoustics*, *133*(6), 061001.

Liu, X.-Q., Zhang, H.-Y., Liu, J., & Yang, J. (2000). Fault detection and diagnosis of permanent-magnet DC motor based on parameter estimation and neural network.

IEEE Transactions on Industrial Electronics, *47*(5), 1021–1030.

Mohamad, T. H., Kwuimy, C. K., & Nataraj, C. (2017). Discrimination of multiple faults in bearings using density-based orthogonal functions of the time response. In *Asme 2017 international design engineering technical conferences and computers and information in engineering conference* (pp. V008T12A035–V008T12A035).

Mohamad, T. H., & Nataraj, C. (2017, October). Gear fault diagnostics using extended phase space topology. In *Annual conference of the prognostics and health management society.*

Mohamad, T. H., Samadani, M., & Nataraj, C. (n.d.). Rolling element bearing diagnostics using extended phase space topology. *Journal of Vibration and Acoustics*.

Rabie, M. (2009). *Fluid power engineering*. McGraw Hill Professional.

Samadani, M., Behbahani, S., & Nataraj, C. (2013). A reliability-based manufacturing process planning method for the components of a complex mechatronic system. *Applied Mathematical Modelling*, *37*(24), 9829–9845.

Samadani, M., Kwuimy, C. A., & Nataraj, C. (2014). Fault detection and severity analysis of servo valves using recurrence quantification analysis. In *Annual conference of the prognostics and health management society.*

Samadani, M., Kwuimy, C. K., & Nataraj, C. (2013). Diagnostics of a nonlinear pendulum using computational intelligence. In *Asme 2013 dynamic systems and control conference.*

Samadani, M., Kwuimy, C. K., & Nataraj, C. (2015). Model-based fault diagnostics of nonlinear systems using the features of the phase space response. *Communications in Nonlinear Science and Numerical Simulation*, *20*(2), 583–593.

Samadani, M., Mohamad, T. H., & Nataraj, C. (2016). Feature extraction for bearing diagnostics based on the characterization of orbit plots with orthogonal functions. In *Asme 2016 international design engineering technical conferences and computers and information in engineering conference* (pp. V008T10A026–V008T10A026).